THE JOURNAL OF BIOLOGICAL CHEMISTRY VOL. 283, NO. 41, pp. 27871–27880, October 10, 2008

Lysobisphosphatidic Acid Controls Endosomal Cholesterol Levels*[S]

Received for publication, February 22, 2008, and in revised form, July 7, 2008 Published, JBC Papers in Press, July 21, 2008, DOI 10.1074/jbc.M801463200

Julien Chevallier[‡1,2], Zeina Chamoun[‡1], Guowei Jiang[§], Glenn Prestwich[§], Naomi Sakai[¶], Stefan Matile[§], Robert G. Parton[‖], and Jean Gruenberg[‡3]

From the Departments of [‡]Biochemistry and [¶]Organic Chemistry, University of Geneva, 30 Quai E. Ansermet, 1211 Geneva 4, Switzerland, the [§]Department of Medicinal Chemistry, University of Utah, Salt Lake City, Utah 84108-1257, and [‖]Institute for Molecular Bioscience and Center for Microscopy and Microanalysis, University of Queensland, Brisbane 4072, Queensland, Australia

Most cell types acquire cholesterol by endocytosis of circulating low density lipoprotein, but little is known about the mechanisms of intra-endosomal cholesterol transport and about the primary cause of its aberrant accumulation in the cholesterol storage disorder Niemann-Pick type C (NPC). Here we report that lysobisphosphatidic acid (LBPA), an unconventional phospholipid that is only detected in late endosomes, regulates endosomal cholesterol levels under the control of Alix/AIP1, which is an LBPA-interacting protein involved in sorting into multivesicular endosomes. We find that Alix down-expression decreases both LBPA levels and the lumenal vesicle content of late endosomes. Cellular cholesterol levels are also decreased, presumably because the storage capacity of endosomes is affected and thus cholesterol clearance accelerated. Both lumenal membranes and cholesterol can be restored in Alix knockdown cells by exogenously added LBPA. Conversely, we also find that LBPA becomes limiting upon pathological cholesterol accumulation in NPC cells, because the addition of exogenous LBPA, but not of LBPA isoforms or analogues, partially reverts the NPC phenotype. We conclude that LBPA controls the cholesterol capacity of endosomes.

Endocytosed proteins and lipids destined for degradation, such as down-regulated signaling receptors and LDL,[4] are sequentially transported to early and late endosomes, and eventually to lysosomes. A hallmark of endosomes along this degradation pathway is their multivesicular appearance due to the accumulation of intralumenal vesicles. These incorporate down-regulated receptors (1, 2) and cholesterol (3, 4) and also contain large amounts of LBPA (or bis(monoacylglycero)phosphate), which is only detected in late endosomes (5).

In addition to their presence in intralumenal vesicles, LBPA and cholesterol have been linked functionally. Both are affected by sterol carrier protein-2 expression (6). Moreover, LBPA plays a role in cholesterol transport (7). Some relationship between cholesterol and LBPA has also been revealed in the cholesterol storage disorder Niemann-Pick type C caused by mutations in NPC1 or NPC2, whose precise functions are not known (8–10). In tissues from NPC patients, cholesterol accumulation is paralleled by the accumulation of LBPA and other lipids, in particular sphingolipids (8, 10–12). We previously found that LBPA functions may be controlled by Alix, which binds LBPA-containing bilayers (13). Interestingly, Alix is involved in sorting into multivesicular endosomes (14, 15). Moreover, both Alix and LBPA also play a role in intralumenal vesicle fission from and fusion with the endosome limiting membrane (13, 16, 17).

Here we report that Alix down-expression decreases both the lumenal membrane content of late endosomes and their LBPA level, whereas the cellular cholesterol level is reduced, presumably because the endosomal storage capacity is affected. Indeed, the addition of exogenous LBPA to Alix knockdown cells restores both the intralumenal membrane content of late endosomes and the cholesterol level. Conversely, we find that LBPA becomes limiting upon pathological cholesterol accumulation in NPC cells, because the addition of exogenous LBPA, but not of LBPA isoforms or analogues, reverts the NPC phenotype. We conclude that LBPA controls the cholesterol storage capacity of endosomes.

EXPERIMENTAL PROCEDURES

Cells and Reagents—Baby hamster kidney cells (BHK-21), HeLa cells, and NPC skin fibroblasts were maintained as described previously (7), as was the production and purification of vesicular stomatitis virus (VSV Indiana serotype) (18). We previously described the synthesis of enantiopure 2,2′- and 3,3′- dioleoyl-LBPA (13, 19), which can now be obtained from Echelon Biosciences Inc. (Salt Lake City, UT), and of (*R*,*R*)- and (*S*,*S*)-bisether analogues of LBPA (20). Other lipids were purchased from Avanti Polar Lipids, Inc. We also previously described the 6C4 monoclonal antibody against LBPA (5). The monoclonal antibodies against a cytoplasmic (P5D4) (21) or

* This work was supported by the Swiss National Science Foundation and the Telethon (to J. G.) and the Australian National Health and Medical Research Council (to R. G. P.). The costs of publication of this article were defrayed in part by the payment of page charges. This article must therefore be hereby marked "*advertisement*" in accordance with 18 U.S.C. Section 1734 solely to indicate this fact.

[S] The on-line version of this article (available at http://www.jbc.org) contains supplemental Figs. S1–S4.

[1] Both authors contributed equally to this work.

[2] Present address: Anatomy and Cell Biology Dept., 3640 University St., Montreal, Quebec H3A 2B2, Canada.

[3] To whom correspondence should be addressed. Fax: 41-22-379-6470; E-mail: jean.gruenberg@biochem.unige.ch.

[4] The abbreviations used are: LDL, low density lipoprotein; NPC, Niemann-Pick type C; LBPA, lysobisphosphatidic acid; BHK, baby hamster kidney; siRNA, short interfering RNA; ELISA, enzyme-linked immunosorbent assay; HRP, horseradish peroxidase; DOPC, dioleolylphosphatidylcholine; DOPE, dioleolylphosphatidylethanolamine; VSV, vesicular stomatitis virus.

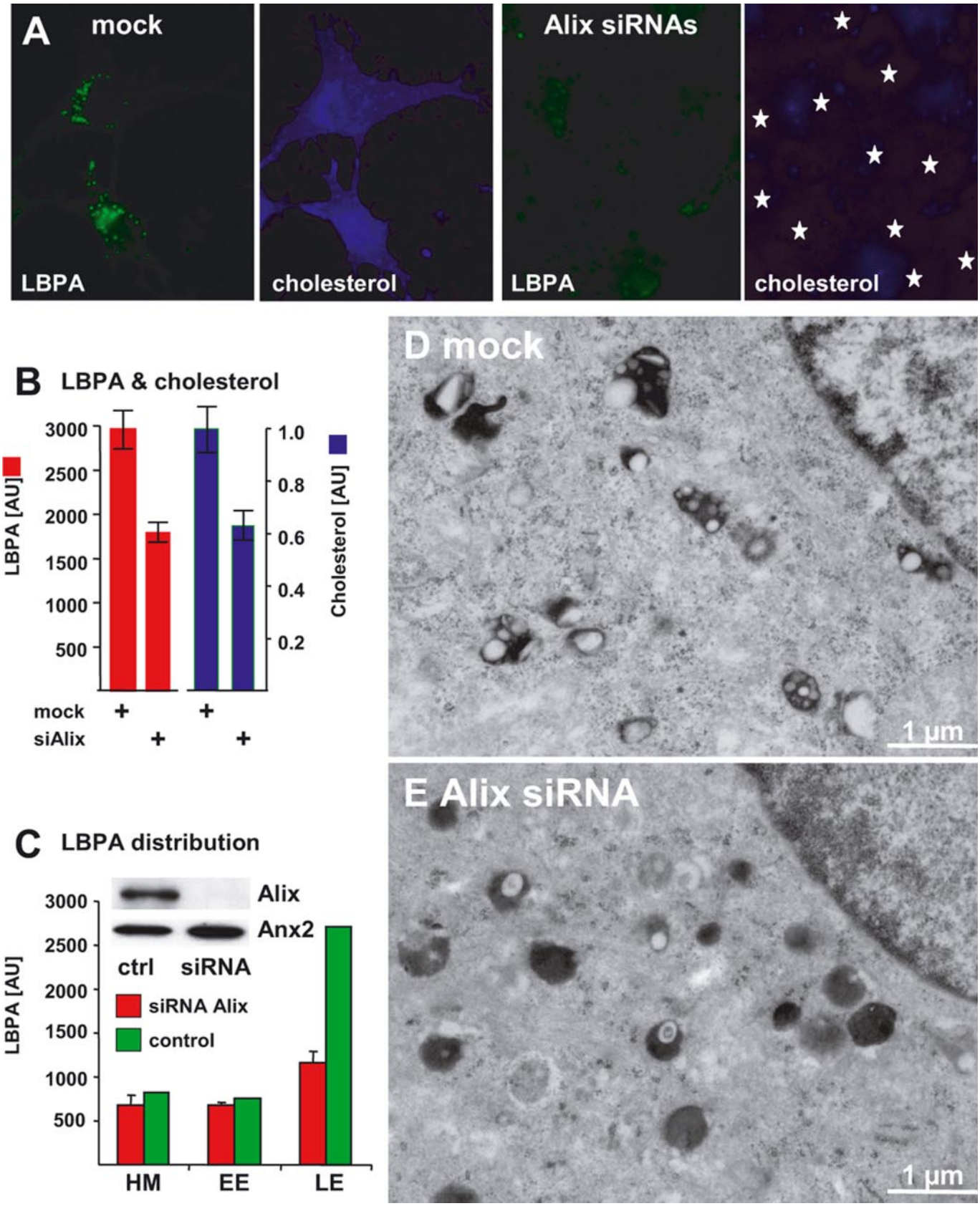

exoplasmic (17.2.21.4) (22) VSV G-protein epitope were described, as well as the polyclonal antibody against G-protein (22). Anti-apolipoprotein A2 was purchased from Biodesign International (Saco, ME). Reagents were obtained from the following sources: anti-mouse Dynabeads from Dynal (Oslo, Norway); *n*-octylpolyoxyethylene from Bachem (Bubendorf, Switzerland); silencer siRNA labeling kit Cy3 from Ambion, Inc. (Huntingdon, UK); fluorescently labeled secondary antibodies from Jackson ImmunoResearch; R18 from Molecular Probes (Eugene, OR); TRIzol from Invitrogen; and U18666A (3-β-[2-(diethylamino)ethoxy]androst-5-en-17-one) from Biomol (Plymouth Meeting, PA).

Analysis of the Genomic Sequence of ALIX siRNA Target in Hamster Cells—RNA from BHK or HeLa cells was extracted with TRIzol according to the manufacturer's instructions. Then 0.5 μg of total RNA was used for reverse transcription with Superscript^{TM}RT (Invitrogen) using random hexamer. The transcribed DNA was subjected to TaqMan reverse transcription-PCR using two primers (forward primer, 5′ GGT GCA GCT GAA GAA GAC CT 3′; reverse primer, 5′ CAG GTT CTG CTC TGC AAT 3′). For TaqMan real time PCR, we used the ICycler.IQ^{TM} (Bio-Rad). Specific PCR bands were excised and purified. The DNA was cloned into a TOPO vector, according to the manufacturer's instructions (Invitrogen). TOP10 bacteria were then transformed and grown; DNA was isolated and then sequenced for analysis by Fasteris SA (Geneva, Switzerland).

Microscopy—The analysis of cholesterol distribution after filipin staining by fluorescence microscopy was described, as was the analysis of LBPA (7) or other antigens (17) by immunofluorescence microscopy. To visualize the content of late endosomes by electron microscopy, HRP was endocytosed for 15 min at 37 °C and then chased for 30 min in marker-free medium (18). Cells were then fixed, and HRP was revealed cytochemically with 3,3′-diaminobenzidine as substrate and processed for plastic embedding (23). Micrographs were taken at random across the monolayer, and then sets of micrographs were analyzed in a blind fashion by an independent observer.

Proteoliposomes Containing VSV-G Protein and LBPA—The major LBPA (>90%) isoform in BHK is 2,2′-dioleoyl-LBPA (5, 19, 24). This isoform was synthesized (19) and used to prepare liposomes by reverse phase evaporation with a phospholipid composition (DOPC/DOPE/LBPA, 60:20:20 mol) similar to that of late endosomes, where LBPA normally resides (5). Because living cells do not take up liposomes efficiently, the G-glycoprotein of vesicular stomatitis virus (VSV-G) was incorporated into the liposomes, to increase cell surface binding and targeting to the endocytic pathway. Thus, liposome delivery was independent of the lipid composition.

To prepare the G-protein, purified VSV (800 μg) was sedimented for 2 h at 4 °C in a TLA100.3 centrifuge at 90,000 rpm. The supernatant was carefully discarded. The white pellet was resuspended in 0.6 ml of 0.1% *n*-octylpolyoxyethylene in HBS (20 mM Hepes, pH 7.4, 150 mM NaCl), by 6–8 passages through a yellow tip until the solution became clear. Then the tubes were gently mixed at room temperature on a rotary wheel (4 rpm) (in 0.6 ml) for 1 h to facilitate detergent extraction of the G-protein. The mixture was then centrifuged at 4 °C for 1 h at 50,000 rpm (TLA 100.3) to separate soluble and nonsoluble materials. The supernatants were collected, dialyzed six times against 250 ml of HBS at 4 °C to remove the detergent, and used to prepare proteoliposomes or aliquoted, flash-frozen in liquid N_2, and stored at −90 °C.

Lipsomes were prepared by reverse phase evaporation (13), after dissolving lipids in $CHCl_3$, and mixed at the following molar ratios: DOPC/DOPE (60:40 mol); DOPC/DOPE/cholesterol (60:20:20 mol); DOPC/DOPE/LBPA (60:20:20 mol); and DOPC/GM3 (70:30 mol). Lipids (total ≈10 mg) were then dried under reduced pressure and dissolved in 1.5 ml of water-saturated diethyl ether and 0.5 ml of HBS (aqueous phase) containing ≈50 μg of G-glycoprotein (equivalent to ≈200 μg of VSV with G = 26% of VSV mass). In some experiments, 10 μM R18, a lipophylic fluorescent dye, was added. The mixture was vortexed and then sonicated continuously for 3 min on ice with a probe-type sonicator (Sonifier 250, Branson) set on power 3. Diethyl ether was then evaporated slowly at 600 mbar for 30–60 min under nitrogen flux on a rotatory evaporator, until lipids become oily. Then 1 ml of HBS (containing the fluorescent dye, if necessary) was added, and the solution was evaporated twice for 30 min on a rotatory evaporator at a 500-mbar pressure and then at 300 mbar until no smell of ether was detected, indicating that full reversion had occurred. When needed, we quantified R18 (excitation 560 nm; emission 585 nm) incorporation into liposomes with a SPECTRAmax GEMINI XS spectrophotometer and SOFTmax Pro (Molecular Devices), as described previously (13). When living cells (grown in 6-cm diameter Petri dishes) were treated with liposomes, the growth medium was replaced by 3 ml of Glascow minimum essential medium containing 10 mM Hepes, pH 7.4, and 0.2% bovine serum albumin, which was then complemented with 100 μl of the desired liposome preparation (0.66 mg of total lipid). The same operation was then repeated every 2 h, until the end of the incubation (after 8 h).

FIGURE 1. **Alix and LBPA.** *A,* BHK cells were treated with siRNAs against Alix (siRNA Alix) or mock-treated (control, *ctrl*) for 72 h. Alix siRNAs were identical to those used in human cells (13), because their target region is identical in hamster (see supplemental Fig S1*A*). Cells were then stained with filipin to reveal cholesterol and with antibodies against LBPA, and analyzed by double-channel fluorescence microscopy. LBPA and cholesterol are decreased after Alix knockdown (but both exhibit their characteristic punctate pattern at longer exposure times, not shown). *Stars* indicate the position of cell nuclei. *B,* BHK cells were treated with Alix siRNAs and homogenized. Total cell extracts were prepared, and both LBPA and cholesterol were quantified. Values are expressed as arbitrary units (*AU*). *C,* mock- or Alix siRNA treated BHK cells were fractionated by floatation in a sucrose gradient (50). After centrifugation, heavy membranes (*HM*), early endosomes (*EE*), and late endosome (*LE*) fractions were collected, and the LBPA content of each fraction was quantified by ELISA. The mean of four different experiments is shown. The *inset* shows an analysis by Western blotting using antibodies against Alix or annexin 2 (*Anx2*); annexin 2, which is also involved in endosome membrane dynamics (2), was not affected. *D* and *E,* late endosome content of BHK cells treated with Alix siRNAs (*E*) or mock-treated (*D*) as in *A* was labeled with HRP pulsed for 15 min at 37 °C and chased for 30 min. Cells were then fixed and processed for HRP cytochemistry and embedded in plastic. *Bar,* 1 μm.

To quantify the incorporation of VSV-G and to determine its trans-bilayer orientation, proteoliposomes (prepared by reverse phase evaporation as above) were immunopurified using Dynabeads coated with antibodies against an exoplasmic (17.2.21.4) or cytoplasmic (P5D4) epitope of the G-protein (18). Similarly, we analyzed the antigenicity of LBPA incorporated into liposomes by incubating 50 μl of the liposome preparation with 15 μl of anti-LBPA antibody in 135 μl of HBS for 3 h at 4 °C. Then the antibody bound to liposomes was separated from free antibody by floatation in a step sucrose gradient (17). In each case, samples were analyzed by SDS-gel electrophoresis under nonreducing conditions, followed by Western blotting using a polyclonal antibody against VSV-G to detect the G-protein or anti-mouse antibodies to detect the anti-LBPA antibody.

To determine the pH-dependent fusion properties of liposomes, we used the following: 1) as acceptor, DOPC/DOPE/LBPA (60:20:20) liposomes containing the G-protein; 2) as donor containing R18, liposomes were passed through a PD-10 Sephadex G-25 column (Amersham Biosciences) to remove the nonencapsulated dye R18. Then 100 μl of donor R18-liposomes were mixed at 4 °C with 50 μl of acceptor liposomes and 50 μl of HBS (neutral conditions) or 50 μl of Tris maleic acid, pH 5.6, in 150 mM NaCl (acidic conditions). The temperature was raised to 22 °C, and the emitted fluorescence (excitation, 560; emission 585) was measured over 90 min with a Photon Technology International fluorimeter (710 Photomultiplier system detection and LPS 220 lamp).

Other Methods—SDS-gel electrophoresis (25) and the quantification of LBPA by ELISA (5) and cholesterol (26) were described. Down-regulation of Alix expression in BHK cells with siRNAs was as described in HeLa cells (13) except that cells were split (1/20) the day before the experiment and then again (biochemistry, 1/4; immunofluorescence, 1/20) 48 h after siRNA addition. Gene expression was quantified from HeLa cells submitted or not to Alix siRNAs. For each condition, RNA was purified from two independent 10-cm dishes using the RNeasy minikit (Qiagen). Reverse transcription-PCR was performed using the Superscript II kit (Invitrogen) and oligo(dT) primer (Promega). The following amplification was made on an i-cycler (Bio-Rad) with the Quantitect SYBR Green PCR kit (Qiagen). The Quantitect Primers (Qiagen) for the following genes were used: *SREBPF2, DHC7R, ACTB, HMGCR, SDHA, LDLR,* and *PDCD6IP* (Alix).

RESULTS AND DISCUSSION

Formation of Intralumenal Membranes—To investigate LBPA functions in cholesterol storage and transport, we silenced Alix expression in BHK cells (supplemental Fig. S1*A*), because we had characterized LBPA in these cells. We had determined the atomic composition of the BHK major (>90%) LBPA isoform as 2,2′-dioleoyl-LBPA (supplemental Fig. S1*B*). We had also characterized the subcellular distribution and late endosomal content of LBPA (15 mol % of total phospholipids) in BHK cells (5, 19, 24) (see Fig. 1*C*). Upon Alix knockdown (Fig. 1*C*, *inset*), the LBPA staining intensity was decreased (Fig. 1*A*), as observed by others (27) and us (13) in human cells, as was the LBPA content of late endosomal fractions (Fig. 1*C*).

Because LBPA is a major phospholipid of late endosome lumenal membranes (5) and because it is decreased by Alix knockdown, we wondered whether the ultrastructure of late endosomes was affected in Alix knockdown cells. To this end, the lumen of late endosomes was labeled with endocytosed HRP pulsed for 15 min and then chased for 30 min at 37 °C. Cells were then processed for HRP cytochemistry and electron microscopy, and micrographs taken at random were analyzed in a blind fashion. In control, mock-treated cells, HRP-labeled late endosomes contained numerous lumenal inclusions and vesicles, exhibiting the characteristic multivesicular ultrastructure of this compartment in BHK cells (18) (Fig. 1*D*). By contrast, in Alix knockdown cells, HRP-positive endosomes appeared like empty vacuoles with a few internal vesicles (Fig. 1*E*), consistent with observations that LBPA levels are then reduced (Fig. 1, *A*–*C*). These data agree well with our previous findings that Alix knockdown in HeLa cells reduces LBPA levels and the number of multilamellar late endosomes that are typical for these cells (13).

Alix and Cholesterol—We then investigated whether cholesterol was affected in Alix knockdown cells, because LBPA and cholesterol are linked functionally (6–8, 12) and because LBPA and cholesterol are both present in intralumenal endosomal vesicles, although perhaps in different subpopulations (3, 28). Upon filipin staining of mock-treated control cells, cholesterol was mostly present at the plasma membrane by light microscopy but was also faintly detected in intracellular structures, presumably trans-Golgi network and endosomes (Fig. 1*A*), as expected (8, 29). Strikingly, the overall cholesterol staining intensity decreased in Alix knockdown cells concomitantly with decreased LBPA staining (Fig. 1*A*), and biochemical quantification showed that, much like LBPA, the total cellular cholesterol was then reduced by ≈30% (Fig. 1*B*).

We could rule out the possibility that decreased cholesterol levels were because of an inhibition of LDL endocytosis, because Alix knockdown does not affect endocytosis nor transport along the endocytic pathway toward late endosomes and lysosomes or lysosomal degradation (13, 16, 17, 27, 30). Similarly, Alix knockdown did not seem to affect *de novo* cholesterol synthesis, because the expression of genes involved in cholesterol synthesis and accumulation was unchanged (supplemental Fig. S2). Alternatively, Alix down-expression, with a concomitant depletion of LBPA (Fig. 1, *A*–*C*) and loss of lumenal membranes (Fig. 1*E*), may affect the capacity of multivesicular endosomes to store or retain cholesterol. This may affect NPC1 functions in cholesterol transport, because NPC1 is normally present both in intralumenal vesicles and on the limiting membrane of multivesicular endosomes (31). In turn, this may alter cellular cholesterol levels, because endosomal and cellular cholesterol levels are interdependent (29). Upon release from endosomes, perhaps via NPC1 and NPC2, as well as ABCA1 (32) or other members of this protein superfamily (33), cholesterol is rapidly transported to the cell surface (34–36) by vesicular and nonvesicular routes (29). Efflux into the medium and capture by serum carriers, including high density lipoprotein (37) can then occur. We could not measure cholesterol in the medium, because of the necessary presence of fetal calf serum in these RNA interference experiments. However, we hypoth-

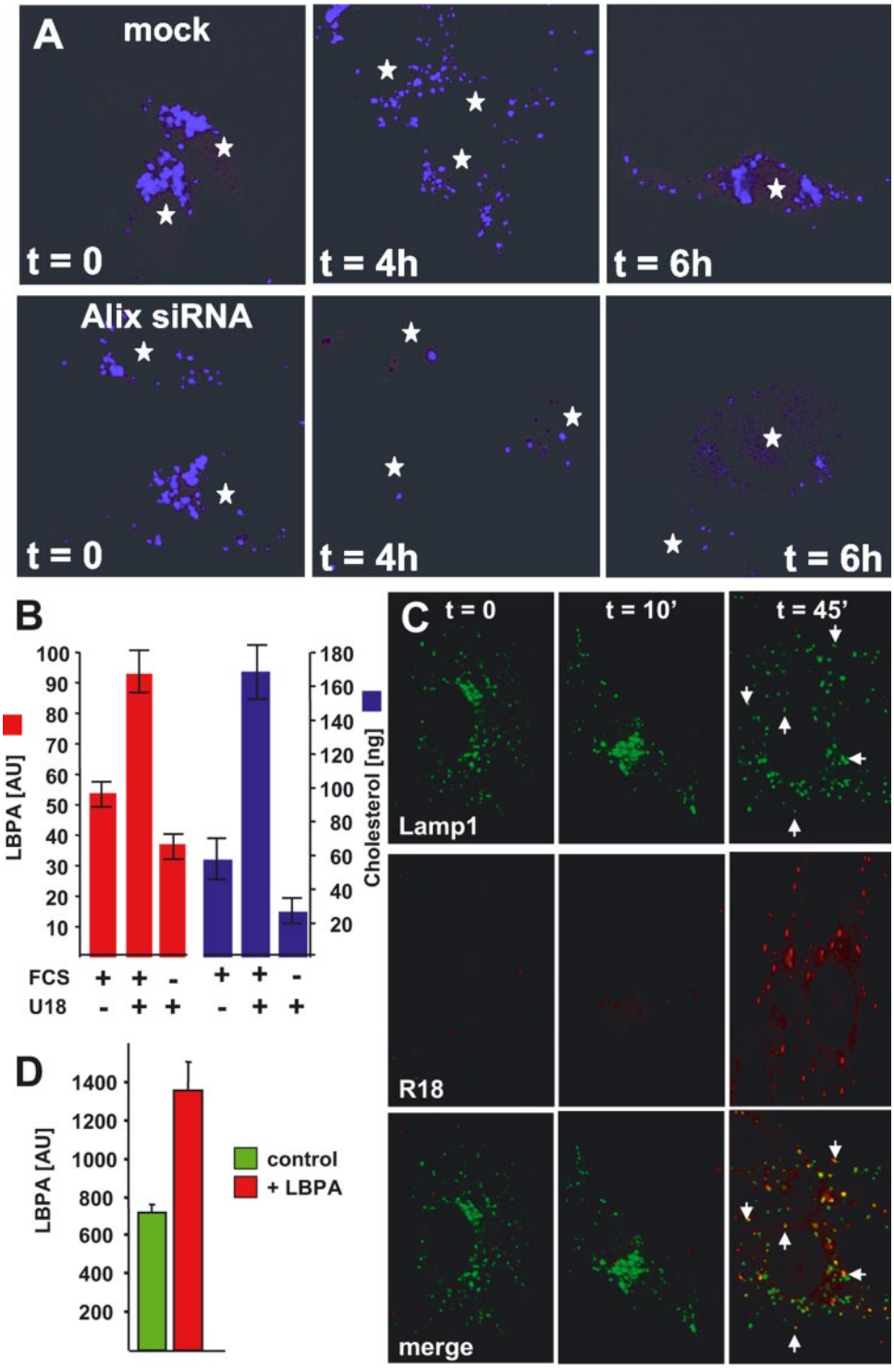

FIGURE 2. **Alix and cholesterol.** *A,* mock-treated or Alix siRNA-treated BHK cells were treated with U18666A for 16 h. The drug was removed, and cells were further incubated in drug-free medium for the indicated times. Cells were labeled with filipin and analyzed by fluorescence microscopy. *Stars* indicate the position of cell nuclei. *A* and *B*, mean of five different experiments is shown. *B,* BHK cells were incubated with or without fetal calf serum and then treated with or without U18666A, as indicated. The total amounts of LBPA (arbitrary units (*AU*)) and cholesterol (ng) in the fractions were quantified. *C,* cells were incubated for 1 h at 4 °C with proteoliposomes containing LBPA and self-quenching amounts of R18 ($t = 0$). Cells were then incubated at 37 °C for the indicated time periods, labeled with antibodies against Lamp1, and visualized by double-channel fluorescence microscopy (*arrowheads* point at examples of structures containing both markers). *D,* total membrane fractions (microsomes) were prepared from BHK cells treated (LBPA) or not (control) with liposomes containing LBPA. The LBPA content of the fractions was then quantified by ELISA and is expressed in arbitrary fluorescence units. The mean of four different experiments is shown.

esized that in the absence of Alix and LBPA, cholesterol may be inefficiently retained in endosomes, and thus cellular clearance may be accelerated.

Cholesterol Accumulation—To test whether Alix and LBPA may play a role in cholesterol clearance from endosomes, we made use of U18666A, a drug that mimics the NPC phenotype by causing acute accumulation of LDL-derived cholesterol in the late endosomes of cells with a nonpathological genetic background (7, 38) (Fig. 2, *A* and *B*). Interestingly, LBPA and cholesterol levels changed concomitantly in U18666A-treated cells. Like cholesterol, LBPA increased in U18666A-treated cells incubated in the presence of serum (Fig. 2*B*). Conversely, cholesterol did not accumulate in U18666A-treated cells incubated in serum-free medium (Fig. 2*B*), as expected (38). LBPA similarly showed no increase in U18666A-treated cells incubated in serum-free medium (Fig. 2*B*), demonstrating that LBPA accumulation in U18666A-treated cells did not result from some effects of the drug on lipid neo-synthesis, and further confirm the notion that LBPA and cholesterol are intimately linked.

Cholesterol accumulated within intracellular vesicles in U18666A-treated cells, as predicted (38) (Fig. 2*A*), which correspond to LBPA-positive late endosomes (Ref. 7) and data not shown). In Alix knockdown cells, accumulation still occurred, albeit with slower kinetics (supplemental Fig. S3), and eventually reached levels comparable with controls (Fig. 2*A*, $t = 0$; after 16 h of U18666A treatment). We then monitored cholesterol clearance from these pre-loaded endosomes after drug washout. The intensity of the cholesterol staining rapidly (over 6 h) decreased in Alix knockdown cells, when compared with controls (Fig. 2*A*). This may suggest that U18666A was less efficiently retained within the endosomes of knockdown cells upon washout. Alternatively, it is possible that cholesterol was more efficiently cleared

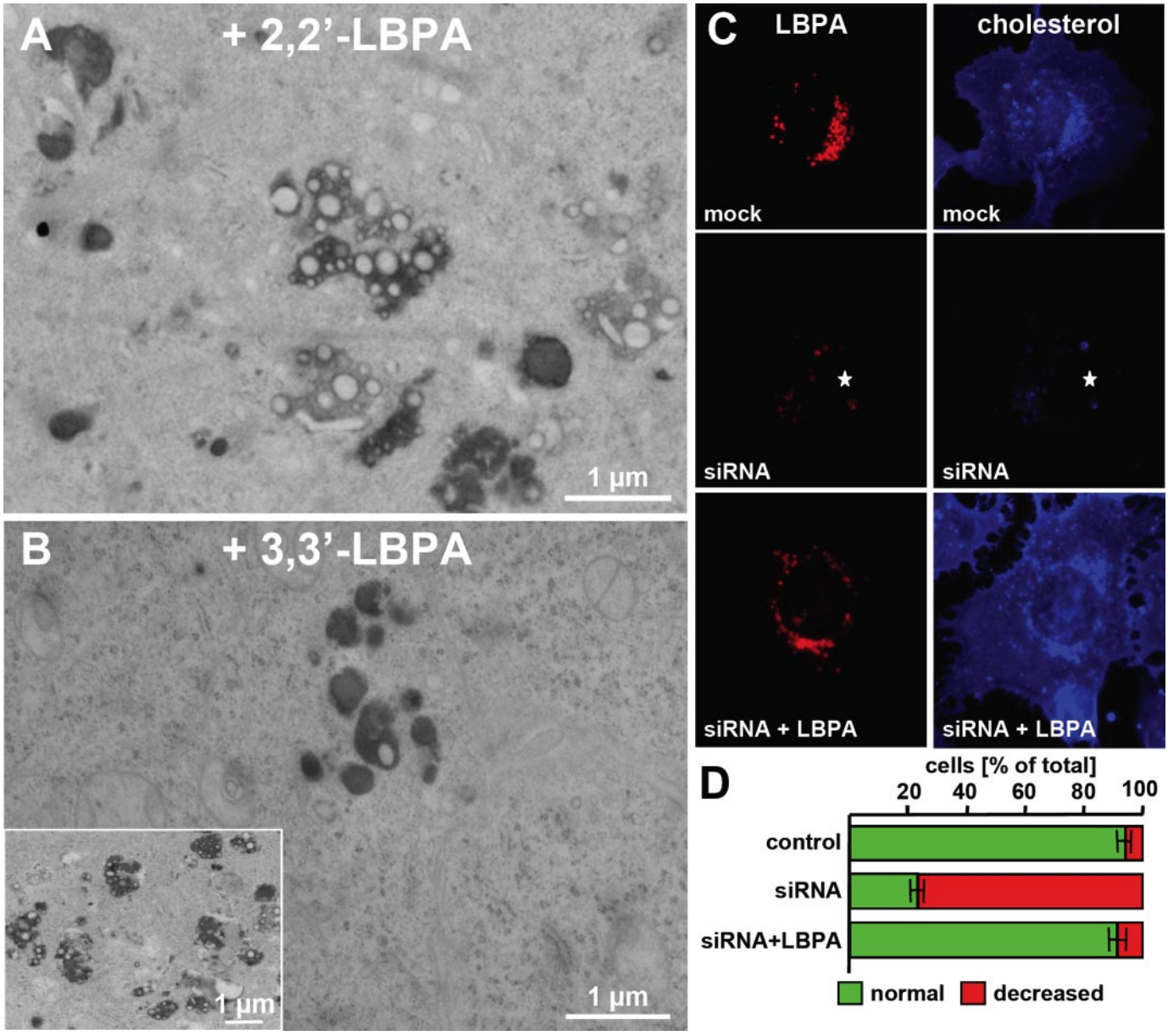

FIGURE 3. **Recomplementation with 3,3′-LBPA.** *A* and *B,* BHK cells treated with Alix siRNAs were incubated as in Fig. 2*C* with proteoliposomes containing 2,2′-dioleoyl-LBPA (*A*) or 3,3′-dioleoyl-LBPA (*B*). Then cells were incubated with HRP to label the late endosome content and processed for electron microscopy, as in Fig. 1, *D–E*. *Bar,* 1 μm. *C* and *D*, cells were treated with Alix siRNA or mock-treated and then with liposomes containing 2,2′-dioleoyl-LBPA (*siRNA + LBPA*), as in *B*, and processed for fluorescence microscopy after staining with anti-LBPA antibodies and filipin to reveal cholesterol (*C*). Filipin staining was significantly reduced after Alix knockdown (*middle panels*), when compared with the mock-treated controls (*upper panels*), and could be restored after recomplementation with 2,2′-dioleoyl-LBPA (*lower panels*). Cells with a reduced or a normal filipin staining pattern were then counted and are expressed (*D*) as a percentage of the total number of cells in each experiment (≈200 cells from three independent experiments).

from endosomes after Alix knockdown, consistent with the notion that Alix and LBPA may be involved in endosomal cholesterol retention.

LBPA Addition Using Liposomes—To further investigate the putative role of Alix and/or LBPA in cholesterol retention, we decided to re-complement Alix siRNA-treated cells with LBPA, using LBPA-containing liposomes. To this end, we synthesized enantiomerically pure (*R*,*R*)-2,2′-dioleoyl-LBPA (19), the major (>90%) isoform in BHK cells (5, 24) (supplemental Fig. S1*B*). The synthetic lipid was then used to prepare liposomes with a phospholipid composition (DOPC/DOPE/LBPA; 60:20:20 mol) similar to that of late endosomes, where LBPA normally resides (5). Because living cells do not take up liposomes efficiently, the G-glycoprotein of vesicular stomatitis virus (VSV-G) was incorporated into the liposomes to increase cell surface binding and targeting to the endocytic pathway (17). The proteoliposomes bound anti-LBPA antibodies but not isotypic control antibodies (supplemental Fig. S4*A*), indicating that LBPA had retained its antigenic properties in the liposome bilayer and was thus presumably present in the same biophysical state as in native membranes. The G-protein was predominantly incorporated in its correct orientation, because liposomes could be immuno-purified with antibodies against an exoplasmic, but not a cytoplasmic, G-protein epitope (supplemental Fig. S4*B*). Finally, these LBPA- and G-containing proteolipo-

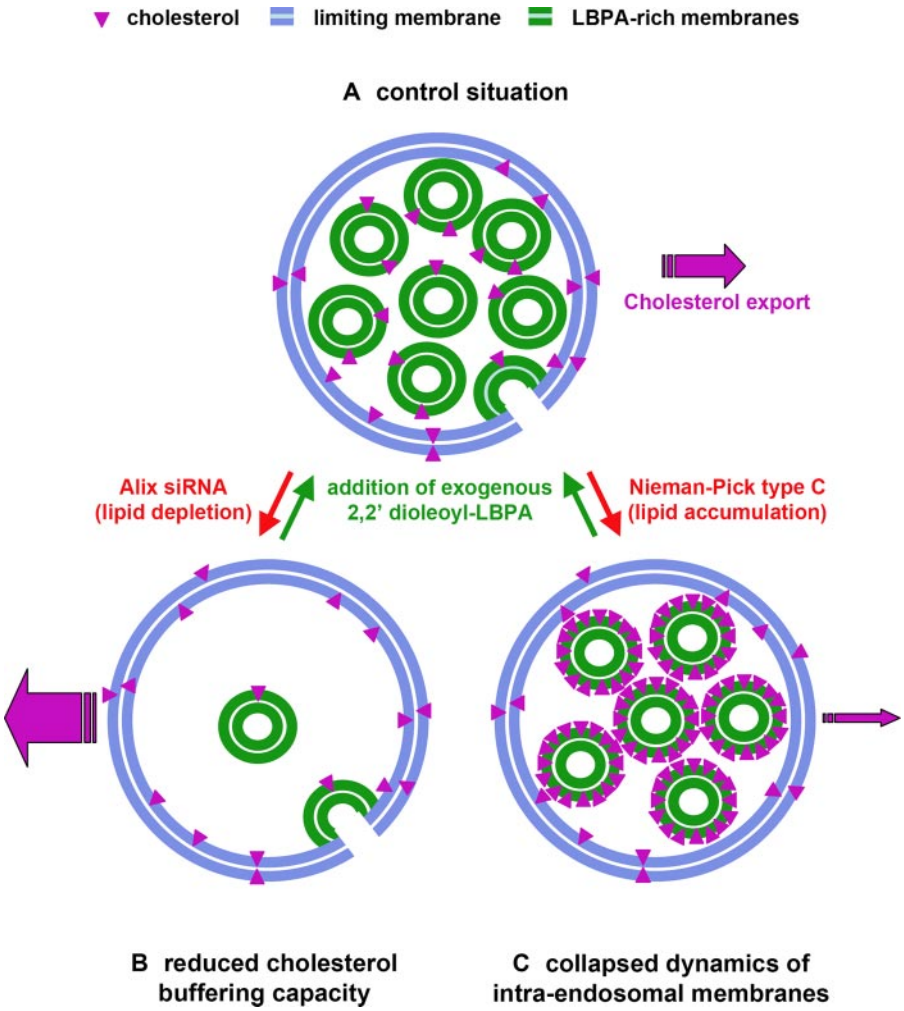

FIGURE 4. **Model.** *A,* under control conditions, LDL-derived cholesterol esters are de-esterified within the lumen of late (multivesicular) endosomes. This releases free cholesterol that, due to its low partition coefficient, is likely to become efficiently incorporated into the closest membranes. These are likely to be predominantly intralumenal membranes, because these are abundant within multivesicular endosomes. Consistently, cholesterol was found to be abundant within intralumenal membranes (3, 4). Cholesterol must be redistributed to the endosome-limiting membrane so that it becomes available for export to other cellular destinations, and this redistribution is likely to involve the back-fusion of intralumenal vesicles (16, 17). *B,* Alix knockdown causes a concomitant reduction in the late endosomal phospholipid LBPA (13). In good agreement with the fact that LBPA is abundant in intralumenal vesicles (5), the late endosomes of Alix knockdown cells are depleted of intralumenal vesicles. Cholesterol clearance seems to be accelerated, presumably because the cholesterol buffering capacity of endosomal membranes is decreased when LBPA and lumenal vesicles are reduced. This notion is further supported by observations that the addition of exogenous LBPA restores both cholesterol levels and intralumenal membranes within late endosomes. *C,* LBPA and other lipids accumulate in NPC cells, concomitantly with an increase in the size of the late endosomal compartment (51), presumably as a compensatory mechanism to accommodate excess cholesterol. Obviously, this mechanism does not suffice to overcome the lipidosis, and eventually cholesterol accumulates beyond the capacity of endosomal membranes, leading to a traffic jam that collapses the endosomal system (40, 41). Consistently, we find that the addition of exogenous LBPA to NPC cells reduces the pathological accumulation of cholesterol, presumably because LBPA became limiting in NPC cells because of cholesterol overload.

somes were highly fusogenic at low pH but not at neutral pH (supplemental Fig. S4*C*), much like VSV itself.

We then tested whether the liposomes containing exogenous LBPA were properly targeted to endosomes. Liposomes were labeled with self-quenching amounts of the fluorescent dye R18, to monitor fusion, and adsorbed onto control BHK cells for 1 h at 4 °C. Cells were then incubated for 45 min at 37 °C and analyzed by immunofluorescence. No fluorescence signal could be detected after liposome binding to the cell surface on ice (Fig. 2*C*). Similarly, no signal was detected when cells were allowed to internalize liposomes for less than 30–45 min at 37 °C (Fig. 2*C* and not shown), demonstrating that dye exchange did not occur to any significant extent under our conditions. At later time points, R18 fluorescent punctae, revealing liposome fusion, appeared intracellularly. These showed a typical late endosome-like pattern and colocalized with both Lamp1 (Fig. 2*C*), a major glycoprotein of late endosomes and lysosomes (39), and with LBPA itself (supplemental Fig. S4*D*). The G-protein showed a similar distribution and colocalized with the late endocytic marker CD63-GFP (24) (supplemental Fig. S4*E*). Using the liposomes, LBPA delivery was successful, because LBPA labeling was more intense and colocalized with Lamp1 (not show) in typical late endosome-like structures (supplemental Fig. S4*D*) and because the total LBPA content of liposome-treated cells increased ≈2-fold (Fig. 2*D*), from ≈1% in control cells (5) to ≈2% of total phospholipids. This increase agrees well with our estimate of the amount of liposomes taken up by cells after G-protein quantification (not shown).

LBPA Recomplementation after Alix Depletion—Alix knockdown causes a concomitant reduction in both LBPA levels (Fig. 1, *A–C*) and lumenal membranes of late endosomes (Fig. 1*E*). We thus used liposomes to recomplement Alix siRNA-treated cells with exogenous LBPA. As in Fig. 1, *D* and *E*, late endosomes were labeled with endocytosed HRP pulsed for 15 min and chased for 30 min at 37 °C. After processing cells for HRP cytochemistry and electron microscopy, micrographs were taken at random and analyzed in a blind fashion. Strikingly, HRP-labeled structures of cells recomplemented with 2,2′-dioleoyl-LBPA, the main LBPA isoform in BHK cells, exhibited the characteristic multivesicular appearance of late endosomes in BHK cells (Fig. 3*A*), which could not be distinguished from the appearance of late endosomes in controls (see Fig. 1*D*). These effects were specific, because recomplementation with the 3,3′-dioleoyl-LBPA isoform did not restore lumenal membranes in late endosomes (Fig. 3*B*), which then resembled the empty endosomes observed in Alix knockdown cells (Fig. 1*E*). The appearance of late endosomes in 3,3′-LBPA-treated cells is

unlikely to result from some undesired effect of this isoform, because cells containing late endosomes with a normal wild type morphology were occasionally seen in the same preparations (Fig. 3*B, inset*), presumably corresponding to untransfected cells. These observations fit nicely with our previous data that 2,2′-dioleoyl-LBPA, but not the 3,3′-iso-

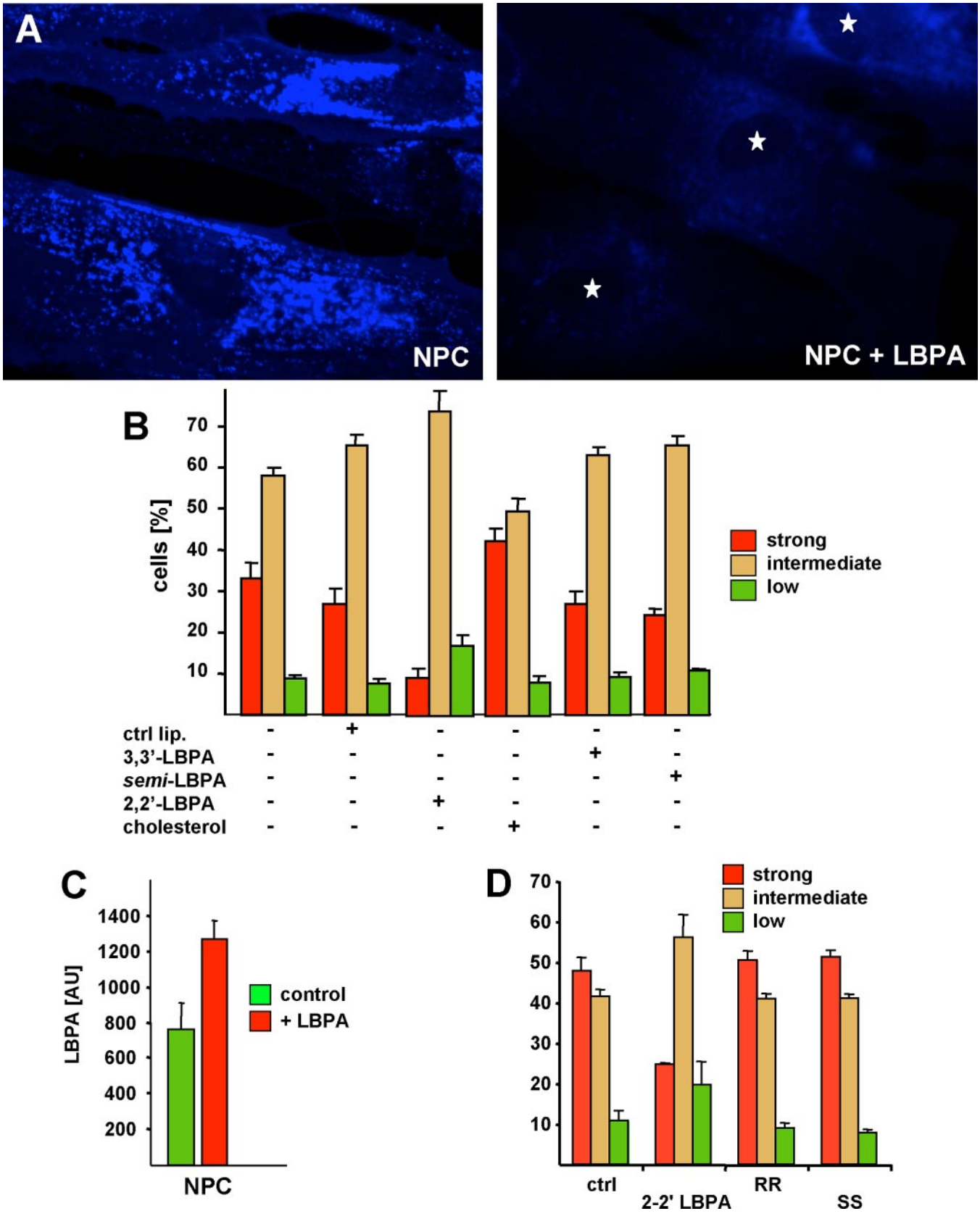

form, can interact with Alix and exhibit the inherent capacity to form multivesicular liposomes *in vitro* (13).

Because addition of exogenous 2,2′-dioleoyl-LBPA could restore lumenal membranes in late endosomes of cells treated with Alix siRNAs, we wondered whether the same treatment might overcome the cholesterol deficiency observed after Alix knockdown (Fig. 1, *A* and *B*). We could not quantify cholesterol directly in these siRNA- and liposome-treated cells, because amounts were limiting. However, an analysis by light microscopy showed that addition of exogenous 2,2′-dioleoyl-LBPA restored the cholesterol distribution observed after filipin staining, much like LBPA itself (Fig. 3*C*; quantification in *D*). Cholesterol staining showed the characteristic pattern observed in controls, presumably corresponding to the plasma membrane, endosomes, and trans-Golgi network (8, 29). These depletion-recomplementation experiments indicate that LBPA plays a direct role in the maintenance of endosomal cholesterol levels. Under physiological conditions, cholesterol accumulates in intralumenal membranes (3, 4), suggesting that free cholesterol, *e.g.* released after LDL endocytosis and de-esterification, is captured by LBPA-rich internal membranes, presumably because these are more abundant than the limiting membrane (5). In siRNA-treated cells, when LBPA levels are decreased and lumenal membranes reduced (Fig. 1), cholesterol may not be efficiently retained in endosomes, leading to increased leakage (see model Fig. 4). By restoring lumenal membranes (Fig. 3*B*), the addition of exogenous LBPA presumably also restores the endosomal capacity to store cholesterol (Fig. 3, *C* and *D*). We thus conclude that LBPA itself plays a direct role in the maintenance of endosomal cholesterol, perhaps because LBPA-rich membranes help buffer membrane cholesterol (Fig. 4).

Niemann-Pick Type C Cholesterol Storage Disorder—The existence of a link between cholesterol storage and LBPA membranes is further supported by observations that LBPA and cholesterol shift in parallel under diverse cellular conditions. Cholesterol decreases when LBPA decreases after Alix knockdown and is restored upon LBPA re-loading. Consistently, both are also decreased upon sterol carrier protein-2 expression (6). Conversely, LBPA accumulates when cholesterol accumulates *in vitro* (Fig. 2*B*) and in NPC cells *in vivo* (12). It may be that cholesterol accumulation and LBPA are not linked functionally in NPC cells. There is, however, a distinct possibility that LBPA and other lipids accumulate in diseased cells as a compensatory mechanism to accommodate excess cholesterol. Obviously, if this is the case, this mechanism does not suffice to overcome the lipidosis; Alix is unlikely to be limiting, because its expression does not change in NPC or U18666A-treated cells (not shown). One might thus speculate that LBPA increases in diseased cells to compensate for cholesterol accumulation, until LBPA production and the endosomal system collapse under cholesterol overload (40, 41). LBPA itself may eventually become limiting in NPC cells (see model Fig. 4). To test this hypothesis, we treated well established 93.41 human NPC skin fibroblasts (42, 43), with LBPA-containing liposomes.

After treatment with proteoliposomes containing LBPA for 8 h at 37 °C, as above (Fig. 2*C* and Fig. 3*C*), LBPA was increased ≈1.6-fold (Fig. 5*C*), a range similar to that observed in BHK cells (Fig. 2*D*). Strikingly, cholesterol accumulation was significantly reduced in most liposome-treated NPC cells (Fig. 5*A*), which then showed an intracellular pattern reminiscent of healthy cells (see Fig. 1*A* and Fig. 3*C*), including fibroblasts (7). To quantify these effects, NPC cells were divided into the following three categories, because of their heterogeneous phenotype: (i) strong accumulation of cholesterol, which sometimes occupied most of the cytoplasm volume; (ii) reduced (intermediate); (iii) low accumulation (Fig. 5, *B* and *D*). (Some differences in the percentages of cells in each category in Fig. 5, *B* and *D,* reflect variations in separate series of experiments presumably because of culture conditions.) LBPA-containing liposomes reduced the number of cells with a strong phenotype ≈2–3-fold, with a concomitant increase in cells with intermediate and mild phenotypes (Fig. 5, *B* and *D*). These effects were specific, because liposomes lacking LBPA were essentially without effects, whereas liposomes that contained 20 mol % cholesterol (DOPC/DOPE/cholesterol, 60:20:20), instead of 20 mol % LBPA, further increased cholesterol levels (Fig. 5*B*).

LBPA Isoforms and Analogues—The observed effects were also specific for the 2,2′-dioleoyl-LBPA isoform, because cholesterol accumulation was not significantly affected by liposomes containing 3,3′-dioleoyl-LBPA or a triple acylated version of the lipid (semi-LBPA) (Fig. 2*A*), which was reported to be present in vaccinia virus and perhaps in the Golgi apparatus (44) (Fig. 5*B*). Hence, esterification of the acyl chains to the 2- and 2′-positions of the glycerol backbone is essential for LBPA function in cholesterol clearance. It is attractive to believe that LBPA functions in cholesterol clearance and endosomal membrane dynamics are linked because 2,2′-LBPA but not 3–3′ LBPA (i) interacts with Alix, (ii) supports the invagination of artificial membranes *in vitro* (13), and (iii) restores lumenal membranes in Alix knockdown cells (Fig. 3*A*).

Because acyl chain addition to the 2- and 2′-positions is essential for LBPA functions, we then investigated whether the 2- and 2′-linking groups were also important. Liposomes containing either the enantiomeric *R,R* or *S,S* form of the bis-ether analogue of (*R,R*)-2,2′-dioleoyl-LBPA (20) (supplemental Fig.

FIGURE 5. **Effects of LBPA-liposomes on NPC cells.** *A,* NPC cells were treated or not with liposomes containing LBPA, as indicated, and cholesterol patterns were visualized after filipin staining by fluorescence microscopy. Exposure times were selected to reveal the intracellular distribution of cholesterol in liposome-treated cells. *B,* NPC cells were treated with the following liposome preparations and analyzed as in *A*: control liposomes without LBPA (*ctrl lip*); liposomes containing 3,3′-dioleoyl-LBPA (*3,3′-LBPA*); liposomes containing 2,2′-dioleoyl LBPA (*2,2′-LBPA*); liposomes containing semi-LBPA; liposomes containing cholesterol. For quantification, cells were divided into three categories according to the intensity of the cholesterol-staining pattern, as indicated. The number of cells in each category is counted and expressed as a percentage of the total cells in the corresponding experiment. *C,* total membrane fractions (microsomes) were prepared from NPC cells treated (LBPA) or not (control) with liposomes containing LBPA. The LBPA content of the fractions was then quantified by ELISA and is expressed in arbitrary fluorescence units. Compare with Fig. 2*D* for values in BHK cells. *D,* NPC cells were treated with the following liposome preparations, analyzed as in *A*, and quantified as in *B*: control liposomes without LBPA (*ctrl lip*); liposomes containing 2,2′-dioleoyl LBPA (*2,2′-LBPA*); liposomes containing (*R,R*)- or (*S,S*)-bis-ether LBPA analogues (bis(3-hydroxy-2(*R*)-*O*-oleyl-*sn*-glycero-1-)phosphate and bis(3-hydroxy-2(*S*)-*O*-oleyl-*sn*-glycero-1-)phosphate, respectively. Differences in the percentages of cells in each category in *B* and *D* presumably reflect variations because of culture conditions in separate series of experiments. *B–D,* mean of at least three independent experiments is shown.

S1*B*) did not show any significant effect when compared with the natural bis-ester lipid (Fig. 5*D*). This further establishes the specificity of 2,2′-LBPA action in cholesterol clearance and demonstrates that acylation to the glycerol backbone via a carbonyl group is required for function. Altogether, these data show that cholesterol clearance from NPC endosomes is facilitated by the addition of exogenous LBPA, indicating that LBPA itself becomes limiting in the disease, presumably because cholesterol has accumulated beyond the capacity of endosomal membranes. Similarly, M87 mutant Chinese hamster ovary cells harbor a mutation in a gene distinct from NPC1 or NPC2 but show NPC-like cholesterol accumulation in late endocytic compartments, perhaps because excessive internalization of LDL cholesterol exceeds the capacity of NPC1-containing late endosomes and leads to cholesterol accumulation (31). Then this pathological accumulation causes a complete traffic jam that collapses the endosomal system (40, 41) and eventually interferes with cholesterol-dependent functions of endosomes (28), including early-to-late endosome transport (45) and late endosome motility (46, 47). It is attractive to speculate that LBPA may play a similar role in other lipidoses that are accompanied by cholesterol accumulation in endosomes and lysosomes (48, 49). In conclusion, our observations indicate that the precise modulation of a specific, natural lipid species in a targeted organelle can lead to the partial reversion of a disease phenotype. The identification of LBPA metabolic enzymes may thus provide new biomedical strategies to overcome some of the problems and defects associated with these storage diseases.

Acknowledgments—We are grateful to Marie-Claire Velluz and Marie-Hélène Beuchat for technical help. We thank Gisou van der Goot for critical reading of the manuscript.

REFERENCES

1. Hurley, J. H., and Emr, S. D. (2006) *Annu. Rev. Biophys. Biomol. Struct.* **35,** 277–298
2. Gruenberg, J., and Stenmark, H. (2004) *Nat. Rev. Mol. Cell Biol.* **5,** 317–323
3. Mobius, W., van Donselaar, E., Ohno-Iwashita, Y., Shimada, Y., Heijnen, H. F., Slot, J. W., and Geuze, H. J. (2003) *Traffic* **4,** 222–231
4. Kolter, T., and Sandhoff, K. (2005) *Annu. Rev. Cell Dev. Biol.* **21,** 81–103
5. Kobayashi, T., Stang, E., Fang, K. S., de Moerloose, P., Parton, R. G., and Gruenberg, J. (1998) *Nature* **392,** 193–197
6. Gallegos, A. M., Atshaves, B. P., Storey, S., Schoer, J., Kier, A. B., and Schroeder, F. (2002) *Chem. Phys. Lipids* **116,** 19–38
7. Kobayashi, T., Beuchat, M. H., Lindsay, M., Frias, S., Palmiter, R. D., Sakuraba, H., Parton, R. G., and Gruenberg, J. (1999) *Nat. Cell Biol.* **1,** 113–118
8. Ikonen, E., and Holtta-Vuori, M. (2004) *Semin. Cell Dev. Biol.* **15,** 445–454
9. Sturley, S. L., Patterson, M. C., Balch, W., and Liscum, L. (2004) *Biochim. Biophys. Acta* **1685,** 83–87
10. Futerman, A. H., and van Meer, G. (2004) *Nat. Rev. Mol. Cell Biol.* **5,** 554–565
11. Vanier, M. T. (1983) *Biochim. Biophys. Acta* **750,** 178–184
12. Vanier, M. T., and Millat, G. (2003) *Clin. Genet.* **64,** 269–281
13. Matsuo, H., Chevallier, J., Mayran, N., Le Blanc, I., Ferguson, C., Faure, J., Blanc, N. S., Matile, S., Dubochet, J., Sadoul, R., Parton, R. G., Vilbois, F., and Gruenberg, J. (2004) *Science* **303,** 531–534
14. Odorizzi, G. (2006) *J. Cell Sci.* **119,** 3025–3032
15. Dikic, I. (2004) *BioEssays* **26,** 604–607
16. Abrami, L., Lindsay, M., Parton, R. G., Leppla, S. H., and van der Goot, F. G. (2004) *J. Cell Biol.* **166,** 645–651
17. Le Blanc, I., Luyet, P.-P., Pons, V., Ferguson, C., Emans, N., Petiot, A., Mayran, N., Demaurex, N., Fauré, J., Sadoul, R., Parton, R. G., and Gruenberg, J. (2005) *Nat. Cell Biol.* **7,** 653–664
18. Gruenberg, J., Griffiths, G., and Howell, K. E. (1989) *J. Cell Biol.* **108,** 1301–1316
19. Chevallier, J., Sakai, N., Robert, F., Kobayashi, T., Gruenberg, J., and Matile, S. (2000) *Org. Lett.* **2,** 1859–1861
20. Jiang, G., Xu, Y., Falguieres, T., Gruenberg, J., and Prestwich, G. D. (2005) *Org. Lett.* **7,** 3837–3840
21. Kreis, T. E. (1986) *EMBO J.* **5,** 931–941
22. Gruenberg, J., and Howell, K. E. (1985) *Eur. J. Cell Biol.* **38,** 312–321
23. Parton, R. G., Schrotz, P., Bucci, C., and Gruenberg, J. (1992) *J. Cell Sci.* **103,** 335–348
24. Kobayashi, T., Beuchat, M. H., Chevallier, J., Makino, A., Mayran, N., Escola, J. M., Lebrand, C., Cosson, P., and Gruenberg, J. (2002) *J. Biol. Chem.* **277,** 32157–32164
25. Laemmli, U. K. (1970) *Nature* **227,** 680–685
26. Gamble, W., Vaughan, M., Kruth, H. S., and Avigan, J. (1978) *J. Lipid Res.* **19,** 1068–1070
27. Cabezas, A., Bache, K. G., Brech, A., and Stenmark, H. (2005) *J. Cell Sci.* **118,** 2625–2635
28. Sobo, K., Chevallier, J., Parton, R. G., Gruenberg, J., and van der Goot, F. G. (2007) *PLoS ONE* **2,** e391
29. Maxfield, F. R., and Tabas, I. (2005) *Nature* **438,** 612–621
30. Schmidt, M. H., Hoeller, D., Yu, J., Furnari, F. B., Cavenee, W. K., Dikic, I., and Bogler, O. (2004) *Mol. Cell. Biol.* **24,** 8981–8993
31. Frolov, A., Srivastava, K., Daphna-Iken, D., Traub, L. M., Schaffer, J. E., and Ory, D. S. (2001) *J. Biol. Chem.* **276,** 46414–46421
32. Neufeld, E. B., Stonik, J. A., Demosky, S. J., Jr., Knapper, C. L., Combs, C. A., Cooney, A., Comly, M., Dwyer, N., Blanchette-Mackie, J., Remaley, A. T., Santamarina-Fojo, S., and Brewer, H. B., Jr. (2004) *J. Biol. Chem.* **279,** 15571–15578
33. Rajagopal, A., and Simon, S. M. (2003) *Mol. Biol. Cell* **14,** 3389–3399
34. Lusa, S., Blom, T. S., Eskelinen, E. L., Kuismanen, E., Mansson, J. E., Simons, K., and Ikonen, E. (2001) *J. Cell Sci.* **114,** 1893–1900
35. Chen, W., Sun, Y., Welch, C., Gorelik, A., Leventhal, A. R., Tabas, I., and Tall, A. R. (2001) *J. Biol. Chem.* **276,** 43564–43569
36. Hao, M., Lin, S. X., Karylowski, O. J., Wustner, D., McGraw, T. E., and Maxfield, F. R. (2002) *J. Biol. Chem.* **277,** 609–617
37. Narita, K., Choudhury, A., Dobrenis, K., Sharma, D. K., Holicky, E. L., Marks, D. L., Walkley, S. U., and Pagano, R. E. (2005) *FASEB J.* **11,** 1558–1560
38. Liscum, L., and Faust, J. R. (1989) *J. Biol. Chem.* **264,** 11796–11806
39. Kornfeld, S., and Mellman, I. (1989) *Annu. Rev. Cell Biol.* **5,** 483–525
40. Liscum, L. (2000) *Traffic* **1,** 218–225
41. Simons, K., and Gruenberg, J. (2000) *Trends Cell Biol.* **10,** 459–462
42. Zhang, M., Dwyer, N. K., Neufeld, E. B., Love, D. C., Cooney, A., Comly, M., Patel, S., Watari, H., Strauss, J. F., III, Pentchev, P. G., Hanover, J. A., and Blanchette-Mackie, E. J. (2001) *J. Biol. Chem.* **276,** 3417–3425
43. Holtta-Vuori, M., Maatta, J., Ullrich, O., Kuismanen, E., and Ikonen, E. (2000) *Curr. Biol.* **10,** 95–98
44. Cluett, E. B., Kuismanen, E., and Machamer, C. E. (1997) *Mol. Biol. Cell* **8,** 2233–2240
45. Mayran, N., Parton, R. G., and Gruenberg, J. (2003) *EMBO J.* **22,** 3242–3253
46. Ko, D. C., Gordon, M. D., Jin, J. Y., and Scott, M. P. (2001) *Mol. Biol. Cell* **12,** 601–614
47. Lebrand, C., Corti, M., Goodson, H., Cosson, P., Cavalli, V., Mayran, N., Faure, J., and Gruenberg, J. (2002) *EMBO J.* **21,** 1289–1300
48. Chen, C.-S., Patterson, M. C., Wheatley, C. L., O'Brien, J. F., and Pagano, R. E. (1999) *Lancet* **354,** 901–905
49. Puri, V., Watanabe, R., Dominguez, M., Sun, X., Wheatley, C. L., Marks, D. L., and Pagano, R. E. (1999) *Nat. Cell Biol.* **1,** 386–388
50. Aniento, F., Emans, N., Griffiths, G., and Gruenberg, J. (1993) *J. Cell Biol.* **123,** 1373–1387
51. Sobo, K., Le Blanc, I., Luyet, P. P., Fivaz, M., Ferguson, C., Parton, R. G., Gruenberg, J., and van der Goot, F. G. (2007) *PLoS ONE* **2,** e851

LYSOBISPHOSPHATIDIC ACID CONTROLS ENDOSOMAL CHOLESTEROL LEVELS

Julien Chevallier, Zeina Chamoun, Guowei Jiang, Glenn Prestwich, Naomi Sakai, Stefan Matile, Robert G. Parton, Jean Gruenberg

LEGENDS OF SUPPLEMENTARY FIGURES

Fig S1. Alix RNAi target sequence and LBPA isoforms. **(A)** Alix sequence in BHK cells was determined by RT-PCR and the 21-mer of the sequence used as target for siRNAs (boxed in red) was determined and found to be identical to the human sequence. **(B)** The chemical composition of the different LBPA isoforms and analogues used in the paper is shown (R is C18:1 in the major 2,2'-LBPA isoform of BHK cells).

Fig S2**.** Alix knockdown does not affect the expression of genes involved in cholesterol synthesis and accumulation. Cells were treated with Alix siRNAs or mock-treated, and the expression of the indicated genes was measured by RT-PCR. DHC: dehydrocholesterol reductase; SREB: sterol regulatory element binding transcription factor 2: LDLR: low density lipoprotein (LDL) receptor; SDH: succinate dehydrogenase subunit A. The data represent the mean of three independent experiments; standard errors of the mean are shown.

Fig S3**.** Cholesterol accumulation after U18666A treatment**.** Mock- or Alix siRNA-treated BHK cells were incubated with U18666A for the indicated time. Cells were labeled with filipin and analyzed by fluorescence microscopy. Before the experiment (t=0h), cells were also labeled with anti-LBPA antibodies, to illustrate the decrease in both LBPA and cholesterol after Alix knockdown (lower panels). Stars indicate the position of cell nuclei, and arrows point at examples of endosomes containing cholesterol.

Fig S4. LBPA-containing liposomes. **(A)** Antibodies against LBPA (anti-LBPA) or an isotypic control antibody (isotypic ctrl) were incubated with LBPA-containing liposomes. Liposome-bound (bound) and free (free) antibody were separated by floatation in a sucrose gradient. Antibody binding was analyzed by SDS gel electrophoresis under non-reducing conditions, followed by western blotting with anti-mouse antibodies (mouse IgG indicated by an arrow). **(B)** Liposomes containing VSV-G were immuno-purified with antibodies against a VSV-G exoplasmic epitope (17.2.21.4 ; exo) or cytoplasmic epitope (P5D4, cyto), and analyzed by SDS gel electrophoresis under non-reducing conditions followed by western blotting with a polyclonal anti VSV-G antibody. Arrows point at the VSV-G doublet. **(C)** The fusion capacity of liposomes containing the G-protein and LBPA (acceptor liposomes) was measured at pH 7.4 or 5.6, by quantifying the dequenching of R18 fluorescence, using R18-contanining liposomes as donor. **(D)** Cells were incubated for 1h at 4°C with proteoliposomes containing LBPA and the G-protein, as well as self-quenching amounts of R18 (as in Fig 2B), and then for 45min at 37°C to allow endocytosis of the bound liposomes to occur. Cells were then labeled with antibodies against LBPA, and visualized by double-channel fluorescence microscopy. All R18-contaning structures also contain LBPA, while LBPA shows a broader distribution presumably because some endosomes contain endogenous LBPA but not R18. **(E)** The experiment was as in (D), except that cells transfected with CD63-GFP were used and that R18 was omitted. Cells were then labeled with antibodies against VSV-G, and visualized by double-channel fluorescence microscopy. In (D-E) arrow point at examples of structures containing both markers.

Fig S1 Chevallier

A

```
CCTGGCCAAGCCGCTGGTGAAGTTCATCCA BHK
CCTGGCCAAGCCGCTGGTGAAGTTCATCCA human (187-216)

GCAGACGTACCCGAGCGGCGGCGAGGAGCA BHK
GCAGACTTACCCAAGCGGCGGGAAGAGCA human (217-246)
```

B

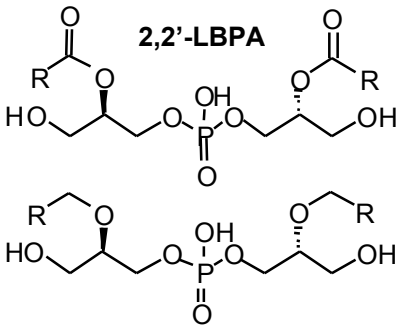

2,2'-bisether LBPA analog

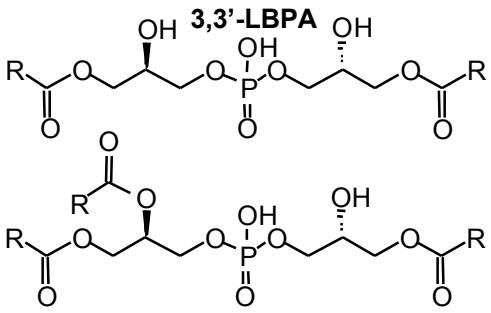

***semi*LBPA**

Fig S2 Chevallier

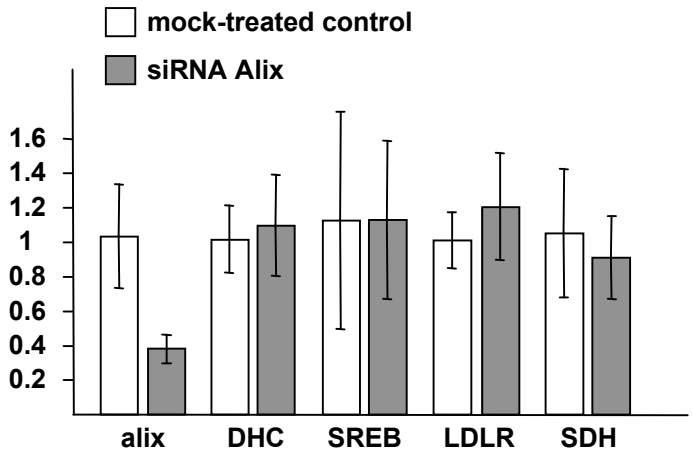

Fig S3 Chevallier

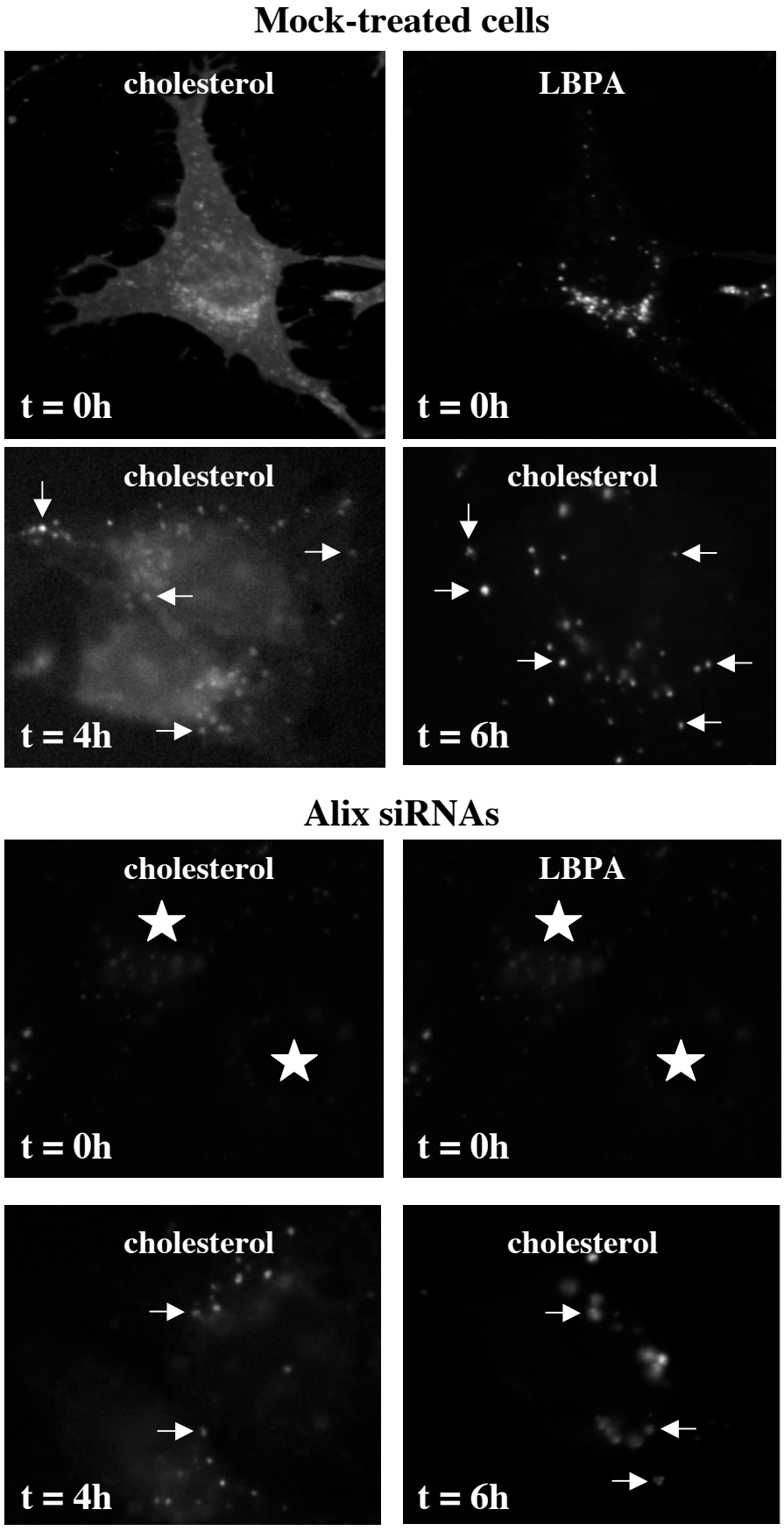

Fig S4 Chevallier

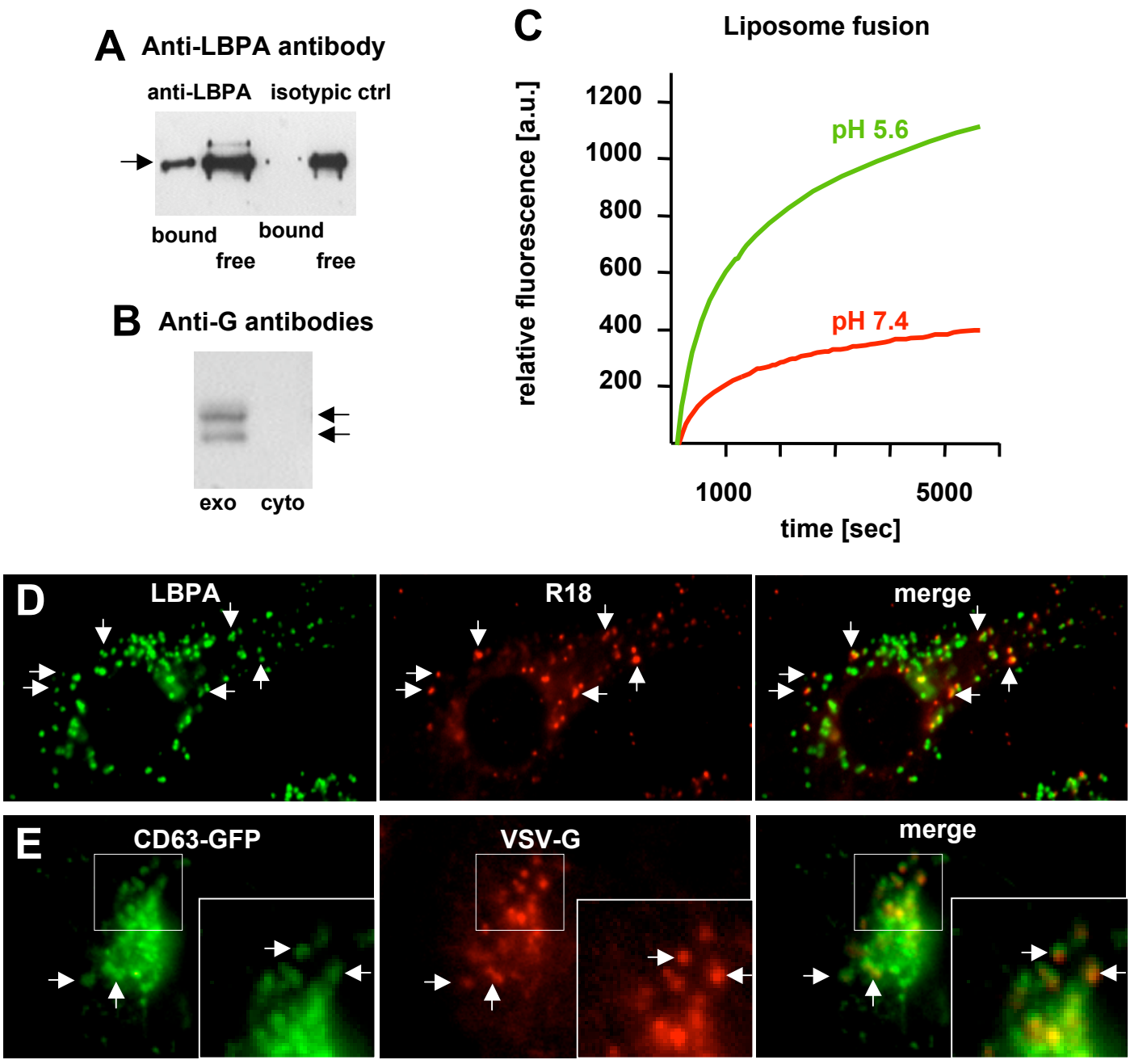

Lysobisphosphatidic Acid Controls Endosomal Cholesterol Levels

Julien Chevallier, Zeina Chamoun, Guowei Jiang, Glenn Prestwich, Naomi Sakai, Stefan Matile, Robert G. Parton and Jean Gruenberg

J. Biol. Chem. 2008, 283:27871-27880.
doi: 10.1074/jbc.M801463200 originally published online July 21, 2008
